JACS
JOURNAL OF THE AMERICAN CHEMICAL SOCIETY

COMMUNICATION

pubs.acs.org/JACS

Chemical Patterning of Ultrathin Polymer Films by Direct-Write Multiphoton Lithography

Hojeong Jeon,[†,⊥] Ray Schmidt,[‡,⊥] Jeremy E. Barton,[‡] David J. Hwang,[†] Lara J. Gamble,[∥] David G. Castner,[∥] Costas P. Grigoropoulos,[*,†] and Kevin E. Healy[*,‡,§]

[†]Laser Thermal Laboratory, Department of Mechanical Engineering, [‡]Department of Bioengineering, and [§]Department of Materials Science and Engineering, University of California, Berkeley, California 94720, United States

[∥]Department of Bioengineering, University of Washington, Seattle, Washington 98185, United States

Supporting Information Web-Enhanced

ABSTRACT: We applied 2-photon laser ablation to write subdiffraction nanoscale chemical patterns into ultrathin polymer films under ambient conditions. Poly(ethylene glycol) methacrylate brush layers were prepared on quartz substrates via surface-initiated atom-transfer radical polymerization and ablated to expose the underlying substrate using the nonlinear 2-photon absorbance of a frequency-doubled Ti:sapphire femtosecond laser. Single-shot ablation thresholds of polymer films were ~1.5 times smaller than that of a quartz substrate, which allowed patterning of nanoscale features without damage to the underlying substrate. At a $1/e^2$ laser spot diameter of 0.86 μm, the features of exposed substrate approached ~80 nm, well below the diffraction limit for 400 nm light. Ablated features were chemically distinct and amenable to chemical modification.

Patterned surface chemistry has been a driver in biological, sensor, optoelectronic, and electronic research for years. During this time parallel patterning techniques such as photolithography, microcontact printing, and imprint lithography have received much attention due to the rapid and relative ease of replicating a pattern.[1−3] Unfortunately, such techniques require master patterns, which are most often generated by expensive direct-write laser patterning mask writers designed for the microelectronics industry.[4] Less elaborate and more readily accessible direct-write approaches such as electron beam lithography (EBL), atomic force microscopy (AFM)-based dip pen nanolithography (DPN), and near-field scanning optical microscopy (NSOM) allow the generation of arbitrary nanoscale patterns, an important feature for most experimental programs focused on nanoscale patterning, but fabrication times are limited by the processing environment and the dose time necessary to generate each feature.[4−6] While such techniques are sufficient for small experimental programs, the cost involved in generating the hundreds of large-area samples with differing geometries needed for ambitious biological and sensor programs is often prohibitive.[7] For this class of applications there is a demonstrated need for rapid direct-write chemical patterning technology with low marginal cost. One potential way to achieve this speed is to extend conventional laser microfabrication technology, by exploiting multiphoton ablation, to reduce feature sizes below the optical diffraction limit.

Multiphoton lithography provides high-resolution material processing requiring neither photomasks nor chemical developers.[8,9] Intense femtosecond laser pulses can induce damage in transparent dielectrics by nonlinear absorption processes such as multiphoton-initiated avalanche ionization.[10] In contrast to material modification by nanosecond or longer laser pulses, there is limited heat exchange during femtosecond laser pulse irradiation, which results in minimizing thermal stress and collateral damage. Therefore, the femtosecond laser-induced ablation process is stable and reproducible.[11,12] In addition, due to the nonlinear optical characteristics and Gaussian beam profile of the femtosecond laser, structures smaller than the processing beam spot size can be fabricated by precisely adjusting the pulse energy close to the ablation threshold.[13,14] Since the laser interaction with dielectric materials is strongly nonlinear, a femtosecond laser focused via far-field optics can achieve ablative features with subwavelength resolution on inorganic (i.e., quartz) and polymer substrates (Figure 1a).[8,13,15] To miniaturize feature sizes in polymeric materials, ultrathin films provide small interaction volumes and promote the formation of nanoscale features.

To produce ultrathin films with the tightly controlled thickness and low surface roughness that are critical in both the formation and characterization of nanoscale features, surface-initiated atom-transfer radical polymerization (SI-ATRP) was used.[16] Because this is a living radical polymerization scheme, SI-ATRP films grow linearly, yield smooth homogeneous films, and leave the terminal unit of the synthesized polymer as an active ATRP initiator, stable even after months on the shelf.[17] In this work 10−80 nm thick polyethyleneglycol monomethacrylate (pEGMA) polymer brush layers, chosen for robust nonfouling behavior, were generated by SI-ATRP on quartz and then ablated by single femtosecond laser pulses to expose the underlying substrate. By processing close to the ablation threshold under multiphoton absorption conditions, patterns with subdiffraction feature diameters were rapidly obtained under ambient conditions in a direct-write method.

To examine the film growth kinetics, the SI-ATRP polymerization was monitored *in situ* using a quartz crystal microbalance with dissipation monitoring (QCM-D). SI-ATRP generates a uniform thin film which grows at ~1 nm/h and yields an average surface roughness of 0.9 nm rms. Addition of Cu(II) ATRP deactivator complex prevented chain termination and ensured a living polymerization.[18] The reaction proceeded linearly with time and then deviated from linearity after ~400 min, as shown in Figure 1b.

Received: January 26, 2011
Published: March 31, 2011

dx.doi.org/10.1021/ja200313q | J. Am. Chem. Soc. 2011, 133, 6138–6141

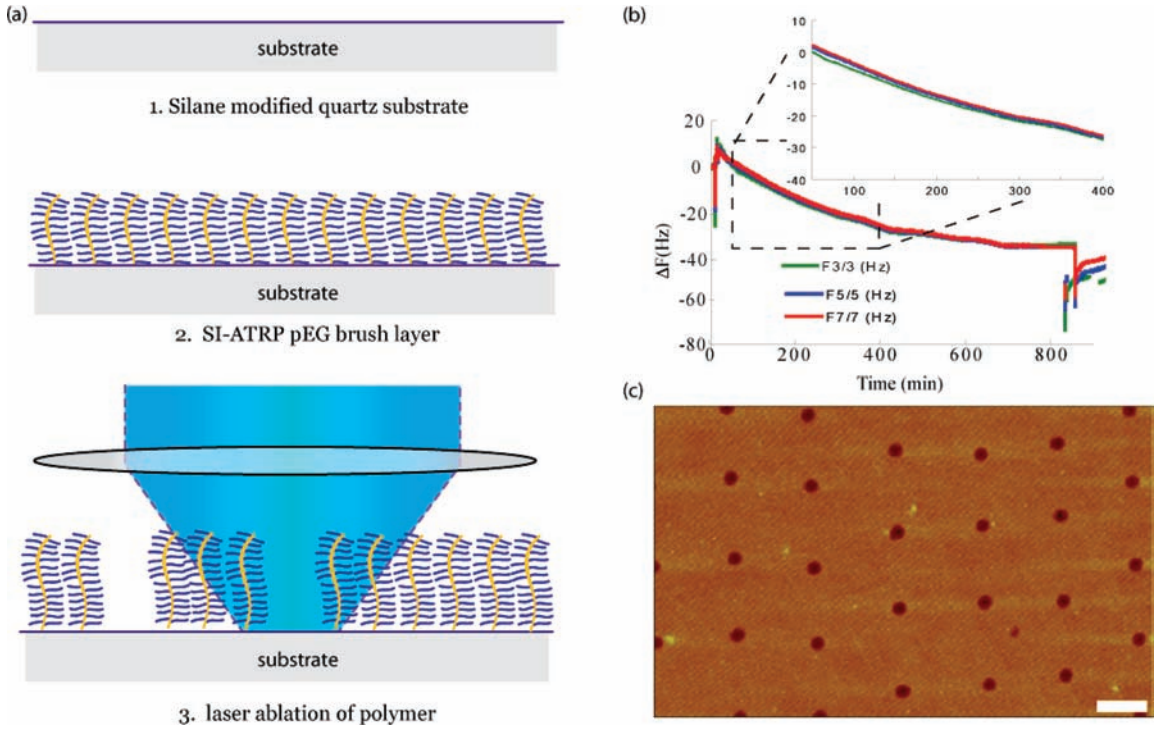

Figure 1. (a) Schematic of laser ablation. Polymer is grown from surface-bound ATRP initiator and ablated by a 100 fs, 400 nm laser pulse. (b) QCM-D measurement of polymer thickness over time indicates linear growth of the living radical polymerization, ensuring the smooth, uniform films necessary for consistent laser ablation. (c) AFM image of 250 nm dot pattern in 20 nm film demonstrates unform feature sizes (scale bar is 1 μm).

The deviation was attributed to deactivation of the catalyst system by slow leakage of oxygen into the QCM-D chamber. Reflectometry measurements of the film thickness revealed a linear increase in film thickness of 1 nm/h for more than 40 h (Figure S1). This linear growth rate provided uniform and controllable polymer films critical for laser ablation experiments. The surface chemistry of the polymer thin film was verified by X-ray photoelectron spectroscopy (XPS). Following growth of a pEGMA brush layer, a large peak resulting from the C−O species was prevalent, verifying the reaction produced a pEGMA film (Figure S2).

Nanoscale features in the pEGMA films were generated by user-designed rastering of a sample through the beam path while applying pulses synchronized with the sample translation. Depending upon the desired pattern arrangement, either single laser pulses were fired by the laser at specified times or a fixed number of pulses were allowed via a mechanical shutter from a train of pulses (maximum frequency 1 kHz) while the translation stage was rastered (details in Supporting Information). To determine the ablation thresholds of both the polymer and the underlying quartz substrate for our particular system, samples were ablated at progressively decreasing pulse energies. The ablation threshold of the pEGMA brush layer was lower than that of the underlying quartz substrate, creating an ideal processing window between 4 and 4.5 nJ. For example, for a 100× objective in which only the 14 nm polymer film was ablated, features of exposed substrate approached ∼80 nm (Figure 2a,b). AFM images of the ablated surfaces, as well as high-resolution images of single features (Figures 1c and 2a), demonstrate the regularity of features at or above 4.5 nJ with a 100× objective.

The processing energy was dependent on the optics of the system (one relevant metric is the numerical aperture), yielding a multiphoton absorption-dependent film ablation threshold energy density of ∼0.8 J/cm^2 with a 100× objective. At pulse energies above 5 nJ, damage to both the pEGMA layer and the underlying quartz substrate was observed (Figure 2b). Using eq 1 (Supporting Information) and the calculated radii of the laser beam (w_0 = 0.43, 0.66, and 2.05 μm for 100×, 50×, and 10× objectives, respectively), the ablation thresholds were calculated to be ∼0.6−1 J/cm^2 for the pEGMA film and ∼1.2−1.5 J/cm^2 for quartz substrate (Figure S2). At fluences between the ablation thresholds of the film and quartz, only the polymer film was removed, exposing the underlying quartz substrate.

The minimum feature sizes depended on the film thickness (Figure 2c): thinner films yielded smaller features, particularly with high NA objectives (Figure S2). This effect was used to generate a wide range of feature sizes by tuning the laser energy and the film thickness. The minimum crater bottom diameters for a 10 nm thick film using 10×, 20×, and 50× objectives were ∼730, ∼370, and ∼160 nm, respectively, and ∼80 nm with a 100× objective for a 14 nm film. This patterning proceeded simply and rapidly at 100−1000 Hz under ambient conditions. While the minimum feature sizes were determined for a single laser shot at a specific wavelength triggering the two-photon absorption process, further improvement in spatial resolution is expected by more rigorous testing with other laser parameters such as number of shots, wavelength, and temporal/spatial beam profiles. Optimization of polymer film characteristics for higher quality of ablation is another route (e.g., one can manipulate the optical, chemical, thermal, and mechanical properties of the film).[19,20] Nevertheless, the wide range of parameters examined in this study supports multiscale feature selectivity with convenient processing windows, either avoiding unwanted substrate damage or exploiting controlled damage for three-dimensional effects.

To verify the localized chemical contrast following ablation of the polymer thin film, the protein Neutravidin was physisorbed

dx.doi.org/10.1021/ja200313q | J. Am. Chem. Soc. 2011, 133, 6138–6141

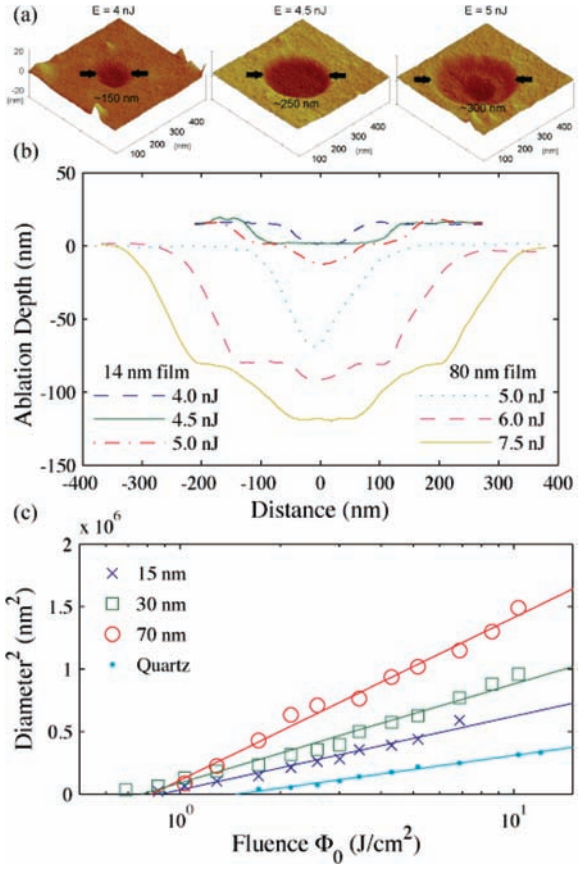

Figure 2. (a) Representative AFM scans of polymer ablation craters in a 14 nm thick film at 4, 4.5, and 5 nJ. In the 5 nJ crater, one can clearly see the ablated quartz in the middle of the feature. (b) Tracing the cross section of features ablated into 14 and 80 nm thick films shows the effect of increasing energy and film thickness very clearly. The 14 nm thick film is offset by 15 nm. (c) For a given objective (100× in this case) and beam profile, the thickness of the film increases the feature size at all energy densities.

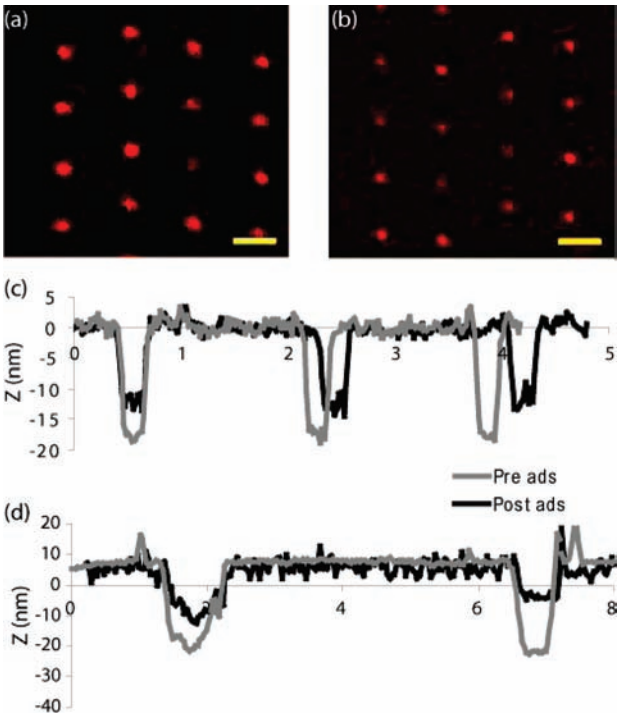

Figure 3. Confocal fluorescence of selectively adsorbed Neutravidin bound to fluorescently labeled biotin in (a) 500 and (b) 300 nm diameter features. Scale bar = 1 μm. AFM cross sections of features before and after (c) Neutravidin and (d) Fibronectin protein adsorption.

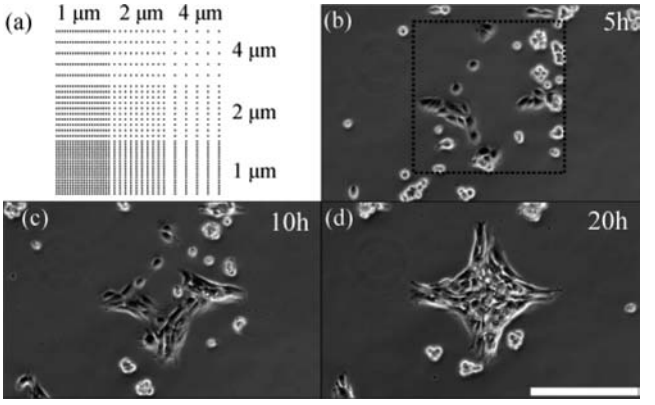

Figure 4. (a) Schematic of the ablated pattern with 500 nm dots on a variable pitch. This diagram shows the inner part of one quadrant of the total pattern, which is mirrored into the other three quadrants around the lower left corner. A more detailed image is given in Figure S4. The pitch between features varied between 1 and 10 μm. (b) 5 h after cells were seeded onto the pattern, they attached and spread on areas of higher density. The dashed box reveals the boundaries of the pattern. (c,d) 10 and 20 h time points that demonstrate robust cell residence only on high-density areas of the pattern with a surface peptide concentration of at least 0.15 pmol/cm^2.

Ⓦ Movie M1 indicates that cells did attach to the low surface density regions and then migrated as either individual cells or cell aggregates to the higher density regions.

to the crater bottom and then tagged with a fluorescently labeled biotin, resulting in patterns shown in Figure 3. Localized regions of fluorescence were observable down to 300 nm diameter features (Figure 3b). Comparing the tapping-mode AFM images of the dried samples before and after protein deposition reveals a 3−4 nm change in the average crater depth, indicating selective protein adsorption (Figure 3c,d). AFM indicated little deposition of protein onto the polymer walls of the crater, suggesting minimal damage to the polymer structure by subthreshold exposure to the femtosecond laser beam and the ejected plume generated by the ablation process.[21]

Finally, we applied this chemical pattering technique to control the adhesion and migration of 3T3-fibroblasts by defining the surface density of ligands for cell surface adhesion receptors (i.e., integrins). We adsorbed Neutravidin protein onto the exposed quartz regions defined by the laser ablation pattern, and we then immobilized onto the nanopatterned protein a biotin-tagged peptide encoding the bone sialoprotein RGD integrin binding domain (bsp-RGD(15): biotin-GGNGEP**RGD**TYRAY).[22] By defining a pattern with a constant 500 nm ablation diameter and varying the pitch between features, we were able to vary the peptide surface density from 2.5 to 0.02 pmol/cm^2. Time-lapse microscopy revealed that seeded cells settled onto the high ligand density region of the gradient, rapidly attached to the surface, and spread, while cells that settled onto the low-density regions of the gradient had difficulty adhering, did not spread significantly, and migrated to the high ligand density regions of the gradient (Figure 4, movie M1, and

Figure S5). Based on the position of the cells after 20 h, which includes both cell adhesion to and migration on the gradient nanopattern, these 3T3-Fibroblast cells preferred a minimal peptide surface density of at least 0.15 pmol/cm^2.

Future developments of this technique will focus on increasing the patterning rate, decreasing the feature size through chemical postprocessing, expanding the pool of polymer materials, and applying the chemistry of the polymer ablation to generate chemical contrast without exposing the underlying quartz. One project of particular interest is to expand the use these patterned substrates to control cell adhesion and explore mechanisms of mechanobiology.

We have determined the chemical, physical, and optical parameters necessary to pattern methacrylate-based polymer thin films at subdiffraction resolutions, and we have applied this system to generate biologically active nanoscale regions of chemical contrast. SI-ATRP provides precise control over the film thickness and uniformity, particularly important parameters for patterning nanoscale features. This first-generation direct-write technique is 1000 times faster than comparable versatile ambient air techniques like DPN and NSOM, and speed, resolution, and material capabilities can be improved in future implementations by using, for example, higher pulse repetition frequency laser sources. Ultimately the high-speed subdiffraction patterning capabilities of femtosecond laser ablation can be combined with the postprocessing potential of SI-ATRP synthesis to produce myriad versatile chemical patterning techniques.

■ ASSOCIATED CONTENT

Ⓢ Supporting Information. Procedures for the synthesis of pEGMA films, laser ablation parameters, and experimental analysis. This material is available free of charge via the Internet at http://pubs.acs.org.

Ⓦ Web Enhanced Feature. A video in .avi format is available in the HTML version of this Communication. Movie M1 shows consecutive phase-contrast images taken for the first 25 h after cell seeding. The play speed is 3000× faster than the real time.

■ AUTHOR INFORMATION

Corresponding Author
cgrigoro@me.berkeley.edu; kehealy@berkeley.edu

Author Contributions
⊥These authors contributed equally.

■ ACKNOWLEDGMENT

National Institutes of Health grants GM085754 and HL096525 are acknowledged (K.E.H., C.P.G.). The XPS experiments were performed at the National ESCA and Surface Analysis Center for Biomedical Problems, which is supported by NIH grant EB-002027 (D.G.C, L.J.G.). We thank Prof. Ting Xu of the Department of Materials Science at the University of California, Berkeley, for use of the Fibermetrics thin-film analyzer.

■ REFERENCES

(1) Lom, B.; Healy, K. E.; Hockberger, P. E. *J. Neurosci. Methods* **1993**, *50*, 385.
(2) Kumar, A.; Whitesides, G. M. *Appl. Phys. Lett.* **1993**, *63*, 2002.
(3) Chou, S. Y.; Krauss, P. R.; Renstrom, P. J. *Science* **1996**, *272*, 85.
(4) Menon, R.; Patel, A.; Gil, D.; Smith, H. I. *Mater. Today* **2005**, *8*, 26.
(5) Piner, R. D.; Zhu, J.; Xu, F.; Hong, S.; Mirkin, C. A. *Science* **1999**, *283*, 661.
(6) Chimmalgi, A.; Hwang, D. J.; Grigoropoulos, C. P. *J. Phys.: Conf. Ser.* **2007**, *59*, 285.
(7) Schmidt, R. C.; Healy, K. E. *J. Biomed. Mater. Res., Part A* **2009**, *90A*, 1252.
(8) Higgins, D. A.; Everett, T. A.; Xie, A. F.; Forman, S. M.; Ito, T. *Appl. Phys. Lett.* **2006**, 88.
(9) Ibrahim, S.; Higgins, D. A.; Ito, T. *Langmuir* **2007**, *23*, 12406.
(10) Grigoropoulos, C. P. *Transport in Laser Microfabrication: Fundamentals and Applications*; Cambridge University Press: New York, 2009.
(11) Chichkov, B. N.; Momma, C.; Nolte, S.; vonAlvensleben, F.; Tunnermann, A. *Appl. Phys. A: Mater. Sci. Processing* **1996**, *63*, 109.
(12) Stuart, B. C.; Feit, M. D.; Rubenchik, A. M.; Shore, B. W.; Perry, M. D. *Phys. Rev. Lett.* **1995**, *74*, 2248.
(13) Korte, F.; Serbin, J.; Koch, J.; Egbert, A.; Fallnich, C.; Ostendorf, A.; Chichkov, B. N. *Appl. Phys. A: Mater. Sci. Processing* **2003**, *77*, 229.
(14) Hwang, D. J.; Grigoropoulos, C. P.; Choi, T. Y. *J. Appl. Phys.* **2006**, 99.
(15) Hartmann, N.; Franzka, S.; Koch, J.; Ostendorf, A.; Chichkov, B. N. *Appl. Phys. Lett.* **2008**, *92*, 3.
(16) Patten, T. E.; Matyjaszewski, K. *Adv. Mater.* **1998**, *10*, 901.
(17) Tugulu, S.; Barbey, R.; Harms, M.; Fricke, M.; Volkmer, D.; Rossi, A.; Klok, H.-A. *Macromolecules* **2006**, *40*, 168.
(18) Pyun, J.; Kowalewski, T.; Matyjaszewski, K. *Macromol. Rapid Commun.* **2003**, *24*, 1043.
(19) Lippert, T.; Hauer, M.; Phipps, C. R.; Wokaun, A. *Appl. Phys. A: Mater. Sci. Processing* **2003**, *77*, 259.
(20) Lippert, T.; Dickinson, J. T. *Chem. Rev.* **2003**, *103*, 453.
(21) Choi, T. Y.; Grigoropoulos, C. P. *J. Appl. Phys.* **2002**, *92*, 4918.
(22) Rezania, A.; Thomas, C. H.; Branger, A. B.; Waters, C. M.; Healy, K. E. *J. Biomed. Mater. Res.* **1997**, *37*, 9.